DYNAMICAL STRUCTURE OF THE MOLECULAR INTERSTELLAR MEDIUM IN AN EXTREMELY BRIGHT, MULTIPLY LENSED $Z\simeq3$ SUBMILLIMETER GALAXY DISCOVERED WITH HERSCHEL

DOMINIK A. RIECHERS[1,28], A. COORAY[2,1], A. OMONT[3], R. NERI[4], A.I. HARRIS[5], A.J. BAKER[6], P. COX[4], D.T. FRAYER[7], J.M. CARPENTER[1], R. AULD[8], H. AUSSEL[9], A. BEELEN[10], R. BLUNDELL[11], J. BOCK[1,12], D. BRISBIN[13], D. BURGARELLA[14], P. CHANIAL[9], S.C. CHAPMAN[15], D.L. CLEMENTS[16], A. CONLEY[17], C.D. DOWELL[12], S. EALES[8], D. FARRAH[18], A. FRANCESCHINI[19], R. GAVAZZI[3], J. GLENN[17], M. GRIFFIN[8], M. GURWELL[11], R.J. IVISON[20,21], S. KIM[2], M. KRIPS[4], A.M.J. MORTIER[16], S.J. OLIVER[18], M.J. PAGE[22], A. PAPAGEORGIOU[8], C.P. PEARSON[23,24], I. PÉREZ-FOURNON[25,26], M. POHLEN[8], J.I. RAWLINGS[22], G. RAYMOND[8], G. RODIGHIERO[19], I.G. ROSEBOOM[18], M. ROWAN-ROBINSON[16], K.S. SCOTT[27], N. SEYMOUR[22], A.J. SMITH[18], M. SYMEONIDIS[22], K.E. TUGWELL[22], M. VACCARI[19], J.D. VIEIRA[1], L. VIGROUX[3], L. WANG[18], J. WARDLOW[2], AND G. WRIGHT[20]

draft version October 10, 2018, accepted for publication in the Astrophysical Journal Letters

ABSTRACT

We report the detection of CO(J=5→4), CO(J=3→2), and CO(J=1→0) emission in the strongly lensed, *Herschel*/SPIRE-selected submillimeter galaxy (SMG) HERMES J105751.1+573027 at z=2.9574±0.0001, using the Plateau de Bure Interferometer, the Combined Array for Research in Millimeter-wave Astronomy, and the Green Bank Telescope. The observations spatially resolve the molecular gas into four lensed images with a maximum separation of ∼9″, and reveal the internal gas dynamics in this system. We derive lensing-corrected CO line luminosities of $L'_{\rm CO(1-0)} = (4.17 \pm 0.41)$, $L'_{\rm CO(3-2)} = (3.96 \pm 0.20)$ and $L'_{\rm CO(5-4)} = (3.45 \pm 0.20) \times 10^{10} \, (\mu_{\rm L}/10.9)^{-1} \, {\rm K \, km \, s^{-1} \, pc^2}$, corresponding to luminosity ratios of r_{31}=0.95±0.10, r_{53}=0.87±0.06, and r_{51}=0.83±0.09. This suggests a total molecular gas mass of $M_{\rm gas}$=3.3×10^{10} $(\alpha_{\rm CO}/0.8) \, (\mu_{\rm L}/10.9)^{-1} \, M_\odot$. The gas mass, gas mass fraction, gas depletion timescale, star formation efficiency, and specific star formation rate are typical for an SMG. The velocity structure of the gas reservoir suggests that the brightest two lensed images are dynamically resolved projections of the same dust-obscured region in the galaxy that are kinematically offset from the unresolved fainter images. The resolved kinematics appear consistent with the complex velocity structure observed in major, 'wet' (i.e., gas-rich) mergers. Major mergers are commonly observed in SMGs, and are likely to be responsible for fueling their intense starbursts at high gas consumption rates. This study demonstrates the level of detail to which galaxies in the early universe can be studied by utilizing the increase in effective spatial resolution and sensitivity provided by gravitational lensing.

Subject headings: galaxies: active — galaxies: starburst — galaxies: formation — galaxies: high-redshift — cosmology: observations — radio lines: galaxies

[1] Astronomy Department, California Institute of Technology, MC 249-17, 1200 East California Boulevard, Pasadena, CA 91125, USA; dr@caltech.edu

[2] Department of Physics & Astronomy, University of California, Irvine, CA 92697, USA

[3] Institut d'Astrophysique de Paris, CNRS and Université Pierre et Marie Curie, 98bis Bd Arago, F-75014 Paris, France

[4] Institut de RadioAstronomie Millimétrique, 300 Rue de la Piscine, Domaine Universitaire, F-38406 Saint Martin d'Héres, France

[5] Department of Astronomy, University of Maryland, College Park, MD 20742-2421, USA

[6] Department of Physics and Astronomy, Rutgers, the State University of New Jersey, 136 Frelinghuysen Road, Piscataway, NJ 08854-8019, USA

[7] National Radio Astronomy Observatory, P.O. Box 2, Green Bank, WV 24944, USA

[8] School of Physics and Astronomy, Cardiff University, Queens Buildings, The Parade, Cardiff CF24 3AA, UK

[9] Laboratoire AIM-Paris-Saclay, CEA/DSM/Irfu - CNRS - Université Paris Diderot, CE-Saclay, pt courrier 131, F-91191 Gif-sur-Yvette, France

[10] Institut d'Astrophysique Spatiale, Université Paris-Sud XI, bât 121, F-91405 Orsay Cedex, France

[11] Harvard-Smithsonian Center for Astrophysics, Cambridge, MA 02138, USA

[12] Jet Propulsion Laboratory, 4800 Oak Grove Drive, Pasadena, CA 91109, USA

[13] Space Science Building, Cornell University, Ithaca, NY,

14853-6801, USA

[14] Laboratoire d'Astrophysique de Marseille, OAMP, Université Aix-marseille, CNRS, 38 rue Frédéric Joliot-Curie, F-13388 Marseille cedex 13, France

[15] Institute of Astronomy, University of Cambridge, Madingley Road, Cambridge CB3 0HA, UK

[16] Astrophysics Group, Imperial College London, Blackett Laboratory, Prince Consort Road, London SW7 2AZ, UK

[17] Dept. of Astrophysical and Planetary Sciences, CASA 389-UCB, University of Colorado, Boulder, CO 80309, USA

[18] Astronomy Centre, Dept. of Physics & Astronomy, University of Sussex, Brighton BN1 9QH, UK

[19] Dipartimento di Astronomia, Università di Padova, vicolo Osservatorio, 3, I-35122 Padova, Italy

[20] UK Astronomy Technology Centre, Royal Observatory, Blackford Hill, Edinburgh EH9 3HJ, UK

[21] Institute for Astronomy, University of Edinburgh, Royal Observatory, Blackford Hill, Edinburgh EH9 3HJ, UK

[22] Mullard Space Science Laboratory, University College London, Holmbury St. Mary, Dorking, Surrey RH5 6NT, UK

[23] Space Science & Technology Department, Rutherford Appleton Laboratory, Chilton, Didcot, Oxfordshire OX11 0QX, UK

[24] Institute for Space Imaging Science, University of Lethbridge, Lethbridge, Alberta, T1K 3M4, Canada

[25] Instituto de Astrofísica de Canarias, E-38200 La Laguna, Tenerife, Spain

[26] Departamento de Astrofísica, Universidad de La Laguna, E-38205 La Laguna, Tenerife, Spain

[27] Department of Physics and Astronomy, University of Penn-

1. INTRODUCTION

Great progress has been made over the past decade in understanding the role of submillimeter-selected galaxies (SMGs; see reviews by Blain et al. 2002; Lagache et al. 2005; Smail 2006) in the early evolution of massive galaxies. Studies of the stellar populations of massive galaxies suggest that they form the bulk of their stars at early epochs ($z>2$), with the more massive galaxies building up their stellar component at earlier epochs and on shorter timescales (see review by Renzini 2006). These findings suggest the existence of a population of massive, gas-rich starburst galaxies at early cosmic times – properties which are consistent with those of SMGs. SMGs are typically intense ($\gtrsim 500\,M_\odot\,\mathrm{yr}^{-1}$), optically obscured, relatively short-lived ($<100\,\mathrm{Myr}$) starbursts at high redshift, implying rapid gas consumption timescales at high star formation efficiencies (e.g., Smail et al. 1997; Hughes et al. 1998; Greve et al. 2005). Most SMGs have sizes of a few kpc and are dynamically complex, exhibiting the properties of gas-rich, major mergers (e.g., Tacconi et al. 2008).

The physical properties of the star-forming material in these extreme galaxies are best studied using rotational emission lines of molecular gas tracers, most commonly CO. Molecular gas is the fuel for star formation, and has been detected in >30 SMGs to date. These typically have large gas reservoirs of $>10^{10}\,M_\odot$ (see review by Solomon & Vanden Bout 2005). The difficulty of such studies is reflected in the moderate number of detections and limited level of detail of most experiments. A promising way to overcome these limitations is to study strongly gravitationally lensed SMGs, as lensing provides a boost in sensitivity and spatial resolution. However, strongly lensed SMGs are very rare, making them difficult to find in typical submillimeter continuum surveys.

With the advent of large area ($\gg 1\,\mathrm{deg}^2$) submillimeter surveys that are currently being undertaken with *Herschel* such as the Multi-tiered Extragalactic Survey (HerMES; S. Oliver et al., in prep.),[29] efficient identification of lensed SMGs is now becoming possible. Here, we study the molecular gas properties of the brightest source identified in these studies.

In this Letter, we report the detection of spatially resolved CO($J=5{\rightarrow}4$) and CO($J=3{\rightarrow}2$) emission and of CO($J=1{\rightarrow}0$) emission toward the strongly lensed SMG HERMES J105751.1+573027 (hereafter: HLSW-01; $z=2.957$), using the Plateau de Bure Interferometer (PdBI), the Combined Array for Research in Millimeter-wave Astronomy (CARMA), and the 100 m Green Bank Telescope (GBT). HLSW-01 was discovered in the HerMES *Herschel*/SPIRE Science Demonstration Phase (SDP) data (Oliver et al. 2010), and is the brightest $z>2$ SMG currently known. Its spectral energy distribution peaks at an (apparent) $250\,\mu\mathrm{m}$ flux of $425{\pm}10\,\mathrm{mJy}$ (Conley et al. 2011; C11). It is lensed by a galaxy group at $z_\mathrm{G}{=}0.60{\pm}0.04$, magnifying the SMG by a factor of $\mu_\mathrm{L}{=}10.9{\pm}0.7$ in flux density (Gavazzi et al. 2011; G11). In accompanying work, we provide additional details on the identification, molecular line excitation (based

on this work and CO $J=7{\rightarrow}6$ to $J=10{\rightarrow}9$ observations with CSO/Z-spec; Scott et al. 2011; S11), spectral energy distribution (C11) and lensing properties (G11) of HLSW-01. We use a concordance, flat ΛCDM cosmology throughout, with $H_0{=}71\,\mathrm{km\,s}^{-1}\,\mathrm{Mpc}^{-1}$, $\Omega_\mathrm{M}{=}0.27$, and $\Omega_\Lambda{=}0.73$ (Spergel et al. 2003, 2007).

2. OBSERVATIONS

2.1. *Plateau de Bure Interferometer*

We observed the CO($J=5{\rightarrow}4$) transition line ($\nu_\mathrm{rest}=576.2679305\,\mathrm{GHz}$, redshifted to $145.633\,\mathrm{GHz}$, or $2.06\,\mathrm{mm}$) toward HLSW-01 ($z=2.957$), using the PdBI. We used the WideX correlator with a total bandwidth of $3.6\,\mathrm{GHz}$ ($\sim 7400\,\mathrm{km\,s}^{-1}$; at $1.95\,\mathrm{MHz}$ resolution) to cover the CO($J=5{\rightarrow}4$) line and the underlying $2\,\mathrm{mm}$ (rest-frame $520\,\mu\mathrm{m}$) continuum emission. Observations were carried out under good $2\,\mathrm{mm}$ weather conditions for 2 tracks in 5D configuration on 2010 June 14 and 17. This resulted in $1.0\,\mathrm{hr}$ of 6 antenna-equivalent on-source time after discarding unusable visibility data. The nearby ($10.6°$ distant) source B0954+658 (J0958+655; $0.98\,\mathrm{Jy}$) was observed every 20 minutes for pointing, amplitude and phase calibration. MWC 349 ($1.50\,\mathrm{Jy}$) and 3C273 ($10.5\,\mathrm{Jy}$) were observed for flux and bandpass calibration, yielding $\sim 10\%$ calibration accuracy.

The IRAM GILDAS package was used for data reduction and analysis. All data were mapped using the CLEAN algorithm with 'natural' weighting, resulting in a synthesized beam of $4.6''{\times}2.8''$. The final rms is $1.2\,\mathrm{mJy\,beam}^{-1}$ over $250\,\mathrm{MHz}$ (corresponding to $515\,\mathrm{km\,s}^{-1}$), $3.4\,\mathrm{mJy\,beam}^{-1}$ over $31.25\,\mathrm{MHz}$ ($64\,\mathrm{km\,s}^{-1}$), and $6.0\,\mathrm{mJy\,beam}^{-1}$ over $10\,\mathrm{MHz}$ ($21\,\mathrm{km\,s}^{-1}$).

2.2. *CARMA*

We observed the CO($J=3{\rightarrow}2$) transition line ($\nu_\mathrm{rest}=345.7959899\,\mathrm{GHz}$, redshifted to $87.388\,\mathrm{GHz}$, or $3.43\,\mathrm{mm}$), using CARMA. A total bandwidth of $3.7\,\mathrm{GHz}$ ($\sim 12{,}700\,\mathrm{km\,s}^{-1}$; at $5.208\,\mathrm{MHz}$ resolution) was used to cover the CO($J=3{\rightarrow}2$) line and the underlying $3.4\,\mathrm{mm}$ (rest-frame $870\,\mu\mathrm{m}$) continuum emission. Observations were carried out under good $3\,\mathrm{mm}$ weather conditions (typically at moderate elevations after transit) for 6 tracks in D configuration between 2010 September 01 and 17. This resulted in $6.6\,\mathrm{hr}$ of 15 antenna-equivalent on-source time after discarding unusable visibility data. The nearby source J0958+655 ($0.86\,\mathrm{Jy}$) was observed every 15 minutes for pointing, amplitude and phase calibration. Fluxes were bootstrapped relative to Mars (based on a brightness temperature model of the planet). Several nearby calibrators (3C84, 3C273, 3C345, J0927+390, J2015+372) were observed for bandpass calibration, yielding $\sim 15\%$ calibration accuracy.

The MIRIAD package was used for data reduction and analysis. All data were mapped using the CLEAN algorithm with 'natural' weighting; resulting in a synthesized beam of $7.7''{\times}5.0''$. The final rms is $0.48\,\mathrm{mJy\,beam}^{-1}$ over $226\,\mathrm{MHz}$ (corresponding to $777\,\mathrm{km\,s}^{-1}$), $1.6\,\mathrm{mJy\,beam}^{-1}$ over $20.8\,\mathrm{MHz}$ ($71\,\mathrm{km\,s}^{-1}$), and $2.3\,\mathrm{mJy\,beam}^{-1}$ over $10.4\,\mathrm{MHz}$ ($36\,\mathrm{km\,s}^{-1}$).

sylvania, Philadelphia, PA 19104, USA
[28] Hubble Fellow
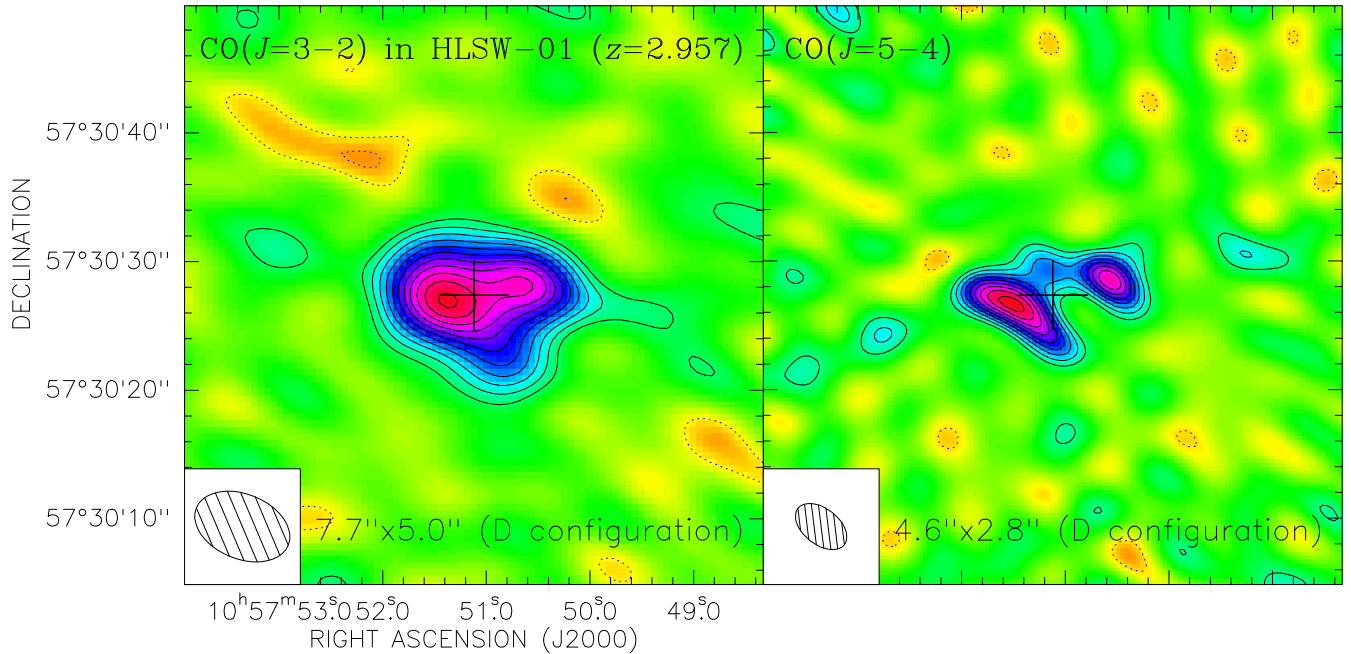[29] http://hermes.sussex.ac.uk/

FIG. 1.— Velocity-integrated CARMA and PdBI maps of CO($J=3 \rightarrow 2$) and CO($J=5 \rightarrow 4$) line emission over 777 and 515 km s^{-1} toward HLSW-01. At $7.7'' \times 5.0''$ and $4.6'' \times 2.8''$ resolution (as indicated in the bottom left), the emission is clearly resolved. The crosses indicate the center of the 250 μm emission (C11). Contours are shown in steps of 1σ=0.48 and 1.2 mJy beam^{-1}, starting at $\pm 2\sigma$.

2.3. GBT

We observed the CO($J=1 \rightarrow 0$) transition line ($\nu_{\rm rest}$ = 115.2712018 GHz, redshifted to 29.131 GHz, or 10.29 mm), using the Zpectrometer analog lag cross-correlation spectrometer (Harris et al. 2007) attached to the GBT Ka band receiver. This yields an instantaneous bandwidth of 10.5 GHz ($\sim$108,000 km s^{-1}) at a beam size of $27''$–$19''$ (25.6–36.1 GHz). Observations were carried out under good 1 cm weather conditions on 2010 October 02. This resulted in 1.5 hr on-source time after discarding unusable data. Subreflector beam switching was used every 10 s to observe the source alternately with the receiver's two beams, with the off-source beam monitoring the sky background in parallel. A nearby second, fainter source was observed with the same pattern, switching between targets with 8 min cycles. Residual structure from optical beam imbalance in the "source–sky" difference spectra of each target was then removed by differencing both sources. A spectral ripple with well-defined period generated in the receiver was removed with narrow-band Fourier filtering. This strategy yields a flat baseline (offset from zero flux by to the difference of the two faint source continua) without standard polynomial baseline removal. The nearby quasar 1143+4931 was observed every $\sim$1 hr to monitor telescope pointing and gain stability. Passband gains and absolute fluxes were determined from spectra of 3C286 (2.04 Jy at 32 GHz; Ott et al. 1994), yielding 15% calibration accuracy.[30]

The lag data were processed using the Zpectrometer's data reduction pipeline and standard recipes, yielding a frequency-calibrated spectrum at 8 MHz resolution (see Harris et al. 2010 for details). The instrumental spectral response is nearly a sinc function with an

[30] The 2010 Astronomical Almanac suggests a slightly lower value of 1.95 Jy at 29 GHz for 3C286.

FWHM of 20 MHz, i.e., individual 8 MHz spectral channels are not statistically independent. However, the line width correction for the instrumental response for spectral lines with intrinsic Gaussian FWHM of $>$30 MHz ($\sim$300 km s^{-1}) is minor.

3. RESULTS

3.1. Integrated Emission Line and Continuum Properties

We have detected spatially resolved CO($J=3 \rightarrow 2$) and CO($J=5 \rightarrow 4$) (Fig. 1) and unresolved CO($J=1 \rightarrow 0$) line emission toward HLSW-01 at high significance. From Gaussian fitting to the (spatially integrated) line profiles (Fig. 2), we obtain CO($J=1 \rightarrow 0$), CO($J=3 \rightarrow 2$), and CO($J=5 \rightarrow 4$) line peak strengths of 3.09$\pm$0.37, 26.4$\pm$1.5 and 64.0$\pm$4.4 mJy at a median FWHM of 348$\pm$18 km s^{-1} (350$\pm$55, 350$\pm$25, and 346$\pm$29 km s^{-1} for the CO $J=1 \rightarrow 0$, $3 \rightarrow 2$, and $5 \rightarrow 4$ lines). We marginally detect 3.43 mm continuum emission under the CO($J=3 \rightarrow 2$) line at 0.61$\pm$0.19 mJy strength, and do not detect 2.06 mm continuum emission down to a 2σ limit of 1.4 mJy. By combining all lines, we find a median redshift of z=2.9574$\pm$0.0001. The line parameters correspond to velocity-integrated emission line strengths of 1.14$\pm$0.11, 9.74$\pm$0.49, and 23.6$\pm$1.4 Jy km s^{-1}, and line luminosities of $L'_{\rm CO(1-0)}$ = (4.17 $\pm$ 0.41), $L'_{\rm CO(3-2)}$ = (3.96 $\pm$ 0.20), and $L'_{\rm CO(5-4)}$ = (3.45 $\pm$ 0.20) $\times$ 10^{10} ($\mu_{\rm L}$/10.9)$^{-1}$ K km s^{-1} pc^2, respectively. This corresponds to line brightness temperature ratios of r_{31}=0.95$\pm$0.10, r_{53}=0.87$\pm$0.06, and r_{51}=0.83$\pm$0.09. This suggests that at least the CO($J=5 \rightarrow 4$) line is not thermalized (i.e., not in radiative equilibrium with the lower-J lines; $r<$1; see also S11). We do not find evidence for a substantial low-excitation gas component in HLSW-01 (i.e., gas with $r_{31} \ll$1), contrary to what is found in some

FIG. 2.— *Left*: CO(J=1→0), CO(J=3→2) and CO(J=5→4) spectra of HLSW-01 at 82/36/21 km s^{-1} (8.0/10.416/10.0 MHz) resolution (histograms), along with Gaussian fits to the line and continuum emission (black curves). The velocity scale is relative to z=2.957. The CO(J=1→0) channels are not statistically independent on scales below 20 MHz (2.5 channels). *Right*: Same, re-binned to similar velocity resolution (82/71/64 km s^{-1}, or 8.0/20.832/31.25 MHz; CO J=1→0 unchanged), and showing a larger velocity range.

other z>2 SMGs (e.g., Carilli et al. 2010; Riechers et al. 2010; Harris et al. 2010; Ivison et al. 2010a). We estimate the total molecular gas mass assuming a conversion factor of α_{CO}=0.8 $M_\odot$ (K km s^{-1} pc^2)$^{-1}$ from $L'_{CO(1-0)}$ to M_{gas}, as appropriate for ultra-luminous infrared galaxies (ULIRGs; Downes & Solomon 1998) and commonly used for SMGs. This yields M_{gas}=3.3×10^{10} $(\alpha_{CO}/0.8)$ $(\mu_L/10.9)^{-1}$ $M_\odot$.

3.2. *Limits on Dense Gas Tracers*

Several lines of dense molecular gas tracers fall within the spectral range covered by the CO(J=3→2) and CO(J=5→4) observations. We obtain 3σ upper limits of <1.6 Jy km s^{-1} on the integrated HCN(J=4→3), CS(J=7→6), SiO(J=8→7), and HC$_3$N(J=39→38) emission line strengths, and <3.2 Jy km s^{-1} for HC$_3$N(J=63→62) and HC$_3$N(J=64→63) (averaged over 348 km s^{-1}). This corresponds to line luminosity limits of <0.61, <0.66, <0.64, <0.61, <0.48, and <0.46 ×10^{10} $(\mu_L/10.9)^{-1}$ K km s^{-1} pc^2 for the HCN, CS, SiO, HC$_3$N(J=39→38), HC$_3$N(J=63→62), and HC$_3$N(J=64→63) lines, respectively. This also corresponds to line brightness temperature ratio limits of <0.15, <0.16, <0.15, <0.15, <0.11, and <0.11 relative to CO(J=1→0). Nearby starburst galaxies and ULIRGs like NGC 253, NGC 6240, and Arp 220 typically have HCN J=4→3/J=1→0 line ratios of 0.45–0.8 (Knudsen et al. 2007; Greve et al. 2009). If this ratio is similar in

HLSW-01, it suggests a HCN/CO ratio of <0.18–0.33 in the respective J=1→0 transitions, consistent with what is found in nearby ULIRGs and other high-z gas-rich galaxies (median ratios of 0.17; Gao & Solomon 2004a, 2004b; Gao et al. 2007; Riechers et al. 2007).

3.3. *Morphology of the Molecular Gas Reservoir*

We spatially resolve the (lensed) molecular gas reservoir in HLSW-01 in the CO(J=3→2) and CO(J=5→4) emission lines. The characteristic effective resolution provided by the lensing effect is ∼2.2″ (i.e., regions of ∼8.5 kpc radius) in CO(J=5→4), but substantially higher in the brighter images and close to critical lines (G11). Overlays of the CO emission with 890 μm (rest-frame 225 μm) continuum emission are shown in Fig. 3. The rest-frame far-infrared (FIR) continuum emission dominantly traces the regions of most active star formation in this system (star formation rate: 2460±160 $(\mu_L/10.9)^{-1}$ $M_\odot$ yr^{-1}; C11). The CO(J=5→4) emission shows discernible peaks at the positions of lens images A, B, and D, with an extension of the emission associated with image B toward image C. Accounting for beam convolution, there is no evidence for differences in the spatial distribution and/or line shapes of the CO(J=3→2) and CO(J=5→4) emission, indicating that both lines trace the same material. The small offsets between the CO and FIR peaks (typically <10% of the relative beam sizes) are a combination of beam convolution (given the different beam sizes and orienta-
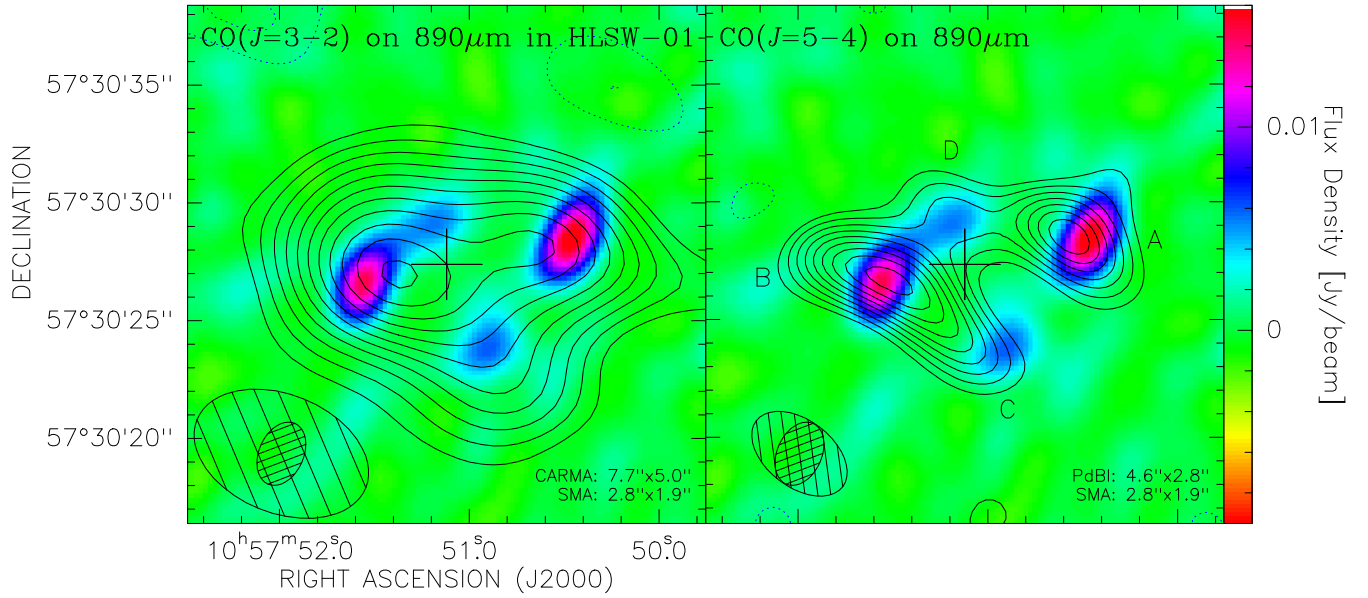
FIG. 3.— CO($J=3\rightarrow2$) and CO($J=5\rightarrow4$) line emission contours as shown in Fig. 1, but overlayed on $890\,\mu$m continuum emission detected with the Submillimeter Array (SMA; color scale; $2.8'' \times 1.9''$ resolution, as indicated in the bottom left; C11). The crosses indicate the same position as in Fig. 1. 'A' to 'D' label the four lensed images of the source ordered by brightness of the $890\,\mu$m continuum emission. CO emission is detected toward all four images.

tions) and velocity-averaged dynamical structure in the integrated molecular line maps. The molecular gas reservoir may extend beyond the FIR continuum peaks, but maps at higher spatial resolution and sensitivity are required to investigate this in more detail. The overall striking match between the gas and (FIR) dust emission suggests that, indeed, the bulk of the FIR light is associated with the gas-rich, star-forming regions.

An overlay of the CO($J=5\rightarrow4$) emission with $2.2\,\mu$m (rest-frame 560 nm; smoothed with a $0.1''$ Gaussian kernel) continuum emission is shown in Fig. 4. The CO emission is clearly associated with the faint optical lensed images of the SMG, which appear to consist of multiple clumps. However, the brightest CO peaks are slightly offset from the peaks of the rest-frame optical emission. This offset translates to $\sim2.4\,$kpc in the source plane after correcting for gravitational magnification (G11). This may indicate that the most gas-rich regions are optically obscured and/or the presence of multiple galaxy components, as commonly observed in SMGs. Also, the FIR-brightest lens image A is the optically faintest image of the galaxy, which lends further support to this picture.

3.4. Dynamical Structure of the Gas Reservoir

A first moment map of the CO($J=5\rightarrow4$) emission is shown in Fig. 5 (clipped below 2σ in each velocity channel, smoothed before detection). There is a clear velocity gradient between images A/B and C/D. The peak of image D is blueshifted by up to ~380 km s^{-1} (relative to zero velocity in Fig. 2). The peak of image C is blended with image B, but is consistent with being redshifted by up to ~150 km s^{-1}. Images A and B peak on the line center. Image A shows a smooth north-south velocity gradient from red to blue, and image B shows a gradient in the opposite direction. This gradient is also seen in CO($J=3\rightarrow2$) emission, indicating that these are likely dynamically resolved lensed images of the same region in the galaxy. Images C and D are consistent with

being unresolved, (in their peaks) kinematically distinct regions in the same galaxy or a companion system. The complexity of the velocity structure is unlikely to be due to distortion of the velocity field by gravitational lensing alone, but would be consistent with the dynamical structure of a major, 'wet' (i.e., gas-rich) merger in progress (e.g., Tacconi et al. 2008; Engel et al. 2010).

Based on the velocity-integrated CO($J=5\rightarrow4$) map shown in Fig. 1, G11 find a half flux radius of $1.1\pm0.5\,$kpc for the CO reservoir in HLSW-01, after correcting for gravitational magnification. However, the structure seen in the CO velocity map indicates that this size estimate may be a lower limit. Thus, different parts of the CO emission may be differentially magnified. However, the lens model by G11 suggests that differential lensing effects are only moderate ($\lesssim25\%$), even out to a radius of $10\,$kpc (their Figure 3), and thus, have a relatively minor effect on the integrated gas properties.

3.5. Physical Properties of the Gas, Dust, and Stellar Components

The minimum time for which the starburst in HLSW-01 can be maintained at its current rate is given by the gas depletion timescale[31] $\tau_{\rm dep}^{0.8}=M_{\rm gas}/{\rm SFR}\sim14\pm2\,$Myr, which is short but within the range of values found for 'typical' SMGs (e.g., Greve et al. 2005).

The ratio between $L_{\rm IR}$ ($\propto$SFR) and $L'_{\rm CO}$ ($\propto M_{\rm gas}$) can be used as a measure of the star formation efficiency. Using $L_{\rm IR}=1.43\pm0.09\times10^{13}\,(\mu_{\rm L}/10.9)^{-1}\,L_\odot$ (C11), we find a ratio of $\sim340\pm40$, comparable to what is found in 'typical' SMGs (e.g., Tacconi et al. 2006; Riechers et al. 2010).

HLSW-01 has a dust mass in the range of $M_{\rm dust}=1.0$–$5.2\times10^8\,(\mu_{\rm L}/10.9)^{-1}\,M_\odot$ (C11; S11). This corresponds to a gas-to-dust mass ratio of $f_{gd}^{0.8}=M_{\rm gas}/M_{\rm dust}=60$–$330$, and is consistent with the range of values found in other SMGs (e.g., Michalowski et al. 2010).
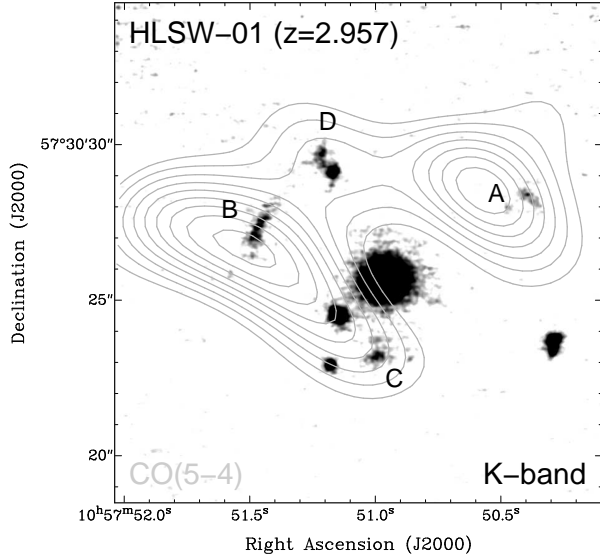
[31] An index '0.8' indicates a linear scaling with $\alpha_{\rm CO}$.

FIG. 4.— CO(J=5→4) line emission contours as shown in Fig. 1, but overlayed on 2.2 μm continuum emission (gray scale; smoothed with a 0.1″ Gaussian kernel; C11). 'A' to 'D' label the four lensed images as in Fig. 3. The CO emission is associated with the four rest-frame optical lensed images, but the peaks of the emission are optically faint.

HLSW-01 has a stellar mass of $M_\star$=6.3±3.4×10^{10} $(\mu_{\rm L}/10.9)^{-1}$ $M_\odot$ (C11), yielding a gas mass fraction of $f_{\rm gas}^{0.8}$=$M_{\rm gas}/M_\star$=0.53±0.29, and a baryonic gas mass fraction of $f_{\rm bary}^{\rm g,0.8}$=$M_{\rm gas}/(M_{\rm gas}+M_\star)$=0.35±0.13. This also yields a specific star formation rate (SSFR, i.e., SFR/$M_\star$) of 39±21 Gyr^{-1}, and a stellar mass doubling timescale ($M_\star$/SFR) of 26±14 Myr. These values are consistent with what is found for other SMGs as well (e.g., Daddi et al. 2009a; Tacconi et al. 2006, 2008).

4. DISCUSSION AND CONCLUSIONS

We have detected spatially resolved, highly excited CO(J=3→2) and CO(J=5→4) emission and CO(J=1→0) emission toward HLSW-01, the 250 μm-brightest SMG found in the HerMES *Herschel*/SPIRE SDP data. Based on these observations, we have refined the redshift of HLSW-01 to z=2.9574±0.0001. Once corrected for lensing magnification, HLSW-01 has a relatively modest molecular gas mass for an SMG. The $M_{\rm gas}$ in HLSW-01 is about twice that found for the strongly lensed z=2.3 SMG J2135−0102 ($M_{\rm gas}$=1.4×10^{10} $(\alpha_{\rm CO}/0.8)$ $(\mu_{\rm L}/32.5)^{-1}$ $M_\odot$; J2135−0102 has ∼0.87 times the apparent 250 μm flux of HLSW-01; Swinbank et al. 2010; Danielson et al. 2011; Ivison et al. 2010b). However, HLSW-01 has a higher CO excitation in its low- to mid-J lines (r_{31}=0.68±0.03, r_{53}=0.51±0.02, and r_{51}=0.35±0.02 in J2135−0102; Danielson et al. 2011). This difference becomes even more dramatic in the high-J CO lines (S11). HLSW-01 also has a higher characteristic dust temperature of 88±3 K (J2135−0102: 30–60 K; Swinbank et al. 2010). The higher CO excitation and dust temperature in HLSW-01 relative to J2135−0102 and other 'typical' z>2 SMGs may be due to a higher relative importance of heating by an active galactic nucleus (AGN), but more detailed studies are required to constrain the presence of an AGN in HLSW-01. The CO line widths,
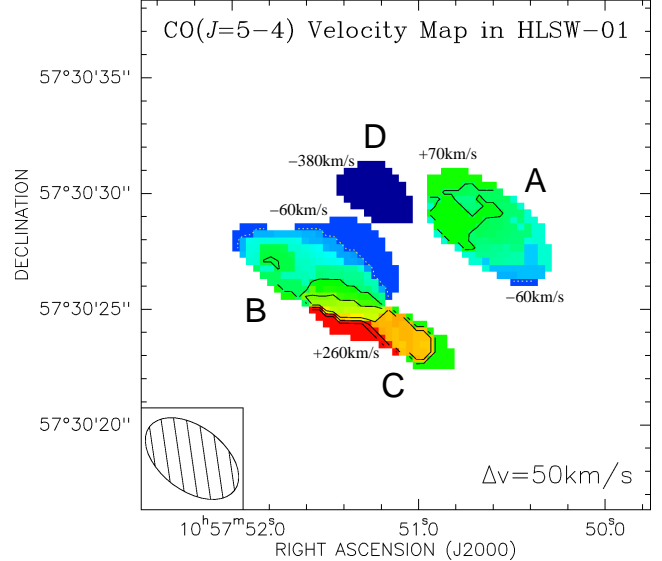

FIG. 5.— CO(J=5→4) first moment map. The colors indicate the velocity gradient. Contours are shown in steps of 50 km s^{-1}, with dotted (solid) contours showing blueshifted (redshifted) emission relative to zero velocity in Fig. 2. 'A' to 'D' label the four lensed images as in Fig. 3. Images A and B are blueshifted relative to image C and redshifted relative to image D. Image A shows a north-south velocity gradient (red to blue), and image B shows a gradient in the opposite direction. No velocity gradients are resolved toward images C and D.

gas depletion timescale, star formation efficiency, (limits on) dense gas fractions, gas-to-dust ratio, gas mass fraction, SSFR, and stellar mass doubling timescale observed toward HLSW-01 are consistent with 'typical' SMGs (e.g., Greve et al. 2005; Gao et al. 2007). The spatial and dynamical structure of the molecular gas reservoir is complex, consistent with what is observed in major mergers in other SMGs (e.g., Tacconi et al. 2008; Carilli et al. 2010; Engel et al. 2010; Bothwell et al. 2010), but higher spatial resolution and a full dynamical lens inversion are required to investigate the velocity structure in more detail (see, e.g., Riechers et al. 2008). The brightest peaks of the CO emission show a small spatial offset from those observed in the rest-frame optical, suggesting that the most gas-rich, most intensely star-forming regions in HLSW-01 are heavily obscured, consistent with what is observed in unlensed SMGs (e.g., Tacconi et al. 2008; Daddi et al. 2009a, 2009b; Carilli et al. 2010; Riechers et al. 2010).

HLSW-01 is an exceptional example for the level of detail to which the molecular gas properties of 'typical' SMGs can be studied with the aid of strong gravitational lensing. Such studies provide crucial insight into the physical processes that accompany the early stellar mass buildup during the most active phases in the evolution of massive galaxies.

REFERENCES

Blain, A. W., et al. 2002, PhR, 369, 111
Bothwell, M. S., et al. 2010, MNRAS, 405, 219
Carilli, C. L., Daddi, E., Riechers, D., et al. 2010, ApJ, 714, 1407
Conley, A., et al. 2011, ApJL, in press [C11]
Daddi, E., et al. 2009a, ApJ, 694, 1517
Daddi, E., et al. 2009b, ApJ, 695, L176
Danielson, A. L. R., et al. 2011, MNRAS, 410, 1687
Downes, D., & Solomon, P. M. 1998, ApJ, 507, 615
Engel, H., et al. 2010, ApJ, 724, 233
Gao, Y., & Solomon, P. M. 2004a, ApJS, 152, 63
Gao, Y., & Solomon, P. M. 2004b, ApJ, 606, 271
Gao, Y., Carilli, C. L., Solomon, P. M., & Vanden Bout, P. A. 2007, ApJ, 660, L93
Gavazzi, R., et al. 2011, ApJ, submitted [G11]
Greve, T. R., et al. 2005, MNRAS, 359, 1165
Greve, T. R., et al. 2009, ApJ, 692, 1432
Harris, A. I., et al. 2007, in *From Z-Machines to ALMA: (Sub)Millimeter Spectroscopy of Galaxies*, ed. A. J. Baker, J. Glenn, A. I. Harris, J. G. Mangum, & M. S. Yun (San Francisco: ASP), 82
Harris, A. I., Baker, A. J., Zonak, S. G., Sharon, C. E., Genzel, R., Rauch, K., Watts, G., & Creager, R. 2010, ApJ, 723, 1139
Hughes, D. H., et al. 1998, Nature, 394, 241
Ivison, R. J., et al. 2010a, MNRAS, 404, 198
Ivison, R. J., et al. 2010b, A&A, 518, L35
Knudsen, K. K., et al. 2007, ApJ, 666, 156
Lagache, G., Puget, J.-L., & Dole, H. 2005, ARA&A, 43, 727
Michalowski, M. J., Watson, D., & Hjorth, J. 2010, ApJ, 712, 942
Oliver, S. J., et al. 2010, A&A, 518, L21
Ott, M., Witzel, A., Quirrenbach, A., Krichbaum, T. P., Standke, K. J., Schalinski, C. J., & Hummel, C. A. 1994, A&A, 284, 331
Renzini, A. 2006, ARA&A, 44, 141
Riechers, D. A., Walter, F., Carilli, C. L., & Bertoldi, F. 2007, ApJ, 671, L13
Riechers, D. A., et al. 2008, ApJ, 686, 851
Riechers, D. A., et al. 2010, ApJ, 720, L131
Scott, K., et al. 2011, ApJ, in press [S11]
Smail, I., Ivison, R. J., & Blain, A. W. 1997, ApJ, 490, L5
Smail, I. 2006, arXiv:astro-ph/0603635
Solomon, P. M., & Vanden Bout, P. A. 2005, ARA&A, 43, 677
Spergel, D. N., et al. 2003, ApJS, 148, 175
Spergel, D. N., et al. 2007, ApJS, 170, 377
Swinbank, A. M., et al. 2010, Nature, 464, 733
Tacconi, L. J., et al. 2006, ApJ, 640, 228
Tacconi, L. J., et al. 2008, ApJ, 680, 246